Front Secondary Crash Management System

Samuel Cardoso
samuel.cardoso@tecnico.ulisboa.pt

Instituto Superior Técnico, Universidade de Lisboa, Portugal

November 2018

Abstract

Over the past 20 years, more than 800,000 people have died on the roads of the European Union. Thanks to the joint effort of some organizations and governments, these numbers have been decreasing due to the creation of regulations to include passive and active protection systems in vehicles. This way, this work was developed to create a structure or several structures that protect the occupants in case of frontal collision in order to be applied in a modular platform that will carry several types of vehicles. Thus, for each case, the structures were developed to protect the occupants regarding the Euro NCAP frontal full width test protocol. The structural development process was based on some geometric parametrization and a multi-objective genetic optimization was used to find the best solutions from the finite element analyses. Four types of vehicles were considered. For the lighter case, a primary structure was developed to absorb the corresponding energy during the impact. The heavier vehicles have a secondary structure to absorb the energy corresponding to the added weight. The final geometries have proven to fulfil the assumptions, obtaining a good relation between the mass increase in these structures and the energy absorption during the impact. On the other hand, the insertion of the secondary structure proved to have satisfactory effects on the overall behaviour during the crash events.

Keywords: frontal collision, multi objective optimization, Euro NCAP, genetic algorithm, secondary system, energy absorption

1. Introduction

Car accidents represent one of the largest problems in human losses in society. In the last twenty years, more than 800,000 people died on the roads of the European Union. Thanks to a joint effort of governments and some organizations, the number of deaths has been declining.

In the last few years, market trends are increasingly pushing the automotive industry toward electric power trains. The most important aspect in an electric car, besides safety, is the autonomy. In this way, the structures developed to be in a vehicle of this type should be as light as possible.

Analysing the statistics, front collisions are the most frequent and fatal type of crash [1], so it is very important to design passive systems such as airbags and bumpers to protect the passengers in case of an accident. In an impact of this type, the most solicited structure is the front bumper. To protect effectively the occupants, this structure needs to be robust and light enough to absorb as much energy as possible.

It is possible to predict the behaviour of the structure in case of impact before the production phase using 3D modelling software and Finite Element Analysis (FEA). This procedure can give the main characteristics of the structure such as energy absorption and decelerations. Through crashworthiness principles, it is possible to have the perception of some errors in the design stage, preventing the propagation of these errors to the production phase.

The development in CEiiA of a modular vehicle with a common platform that includes the chassis, power train, drive train and HVAC led to the need of design an effective absorptive system for the diverse vehicle typologies. Thus, it will be developed different absorbing solutions for vehicles present in table 1.

Table 1: Different vehicle topologies and corresponding weights

Vehicle	Micro Car	Sports Car	Be 2.0	Big Sedan
Mass (kg)	1200	1400	1600	1800

Thus, during this work is developed a process that optimize a given structure automatically taking into account the constraints for the project. The optimized solutions must fulfill the regulations of the Frontal Full Width Impact Assessment from Euro NCAP. For the lighter vehicle, the primary structure design should absorb the correspondent

kinetic energy in the crash test as well as in the case of the vehicles with higher weight, a secondary structure should be designed to complement the energy absorption of the primary structure. The secondary structures must be responsible to lead the impact forces to the superior part of vehicle, namely to pillar A and rooftop regions to release tensions in the lower part of the vehicle preventing damages in this area. In the end, a comparison between the different solutions found for each type of vehicles have to be made in order to perceive the benefits or disadvantages of the secondary structure implementation.

The optimization process will include a multi-objective optimization algorithm coupled with 3D modelling tools and Finite Element Analysis, in order to have the most efficient structure, i.e, with the best energy absorption with lower decelerations during the impact.

2. Background

An analysis was made to find the main regulations regarding frontal impact, crashworthiness principles, material formulation present in the commercial softwares, the inclusion of heat affected zones in the soldering processes and the algorithm used to perform optimizations.

2.1. Regulations

The United Nations Economic Commission for Europe (UNECE), the European regulator has created a procedure regarding front collision, the ECE-R94. In this procedure, several criteria as chest deflection, head performance, thorax performance, chest deflection, abdomen protection and pelvis protection are evaluated to perceive the vehicle safety level.

European New Car Assessment Programme (Euro NCAP) was created to provide an independent safety evaluation of cars sold in Europe. This way, several additional tests are performed beyond European regulation. The tests described in table 2 are performed to evaluate the criteria from UNECE [2].

Table 2: Euro NCAP frontal tests

	Offset-Deformable Barrier	**Full Width Rigid Barrier**
Velocity	64 km/h	50 km/h
Offset	40 %	-

Regarding the full width frontal impact, the criteria used to rate the vehicles about head protection in adults are the Head Injury Criteria (HIC),

$$HIC = (t_2 - t_1)\left(\frac{1}{(t_2 - t_1)}\int_{t_1}^{t_2} a\,dt\right)^{2.5}, \quad (1)$$

where $t_2 - t_1 = 15$ corresponds to the 15 ms interval and a is equal to the acceleration in g, maximum peak acceleration and mean acceleration during 3 milliseconds. The values allowed to have maximum rating score are summarized in table 3.

Table 3: Several criteria for NCAP head injury evaluation

Criteria	**Maximum Value**
HIC_{15}	700
Resultant Acc. 3 msec exceedence	65 g
Resultant peak Acceleration	80 g

2.2. Crashworthiness Principles

The main objective of an efficient crash structure is to absorb the maximum kinetic energy as possible without large decelerations. The main parameters to evaluate the crash performance [3] are the energy absorption (EA) given by

$$EA = \int_0^{\delta} F(x)\,dx, \quad (2)$$

the average crush force (F_{av}),

$$F_{av} = \frac{EA}{\delta}, \quad (3)$$

the specific energy absorption (SEA) given as

$$SEA = \frac{EA}{M}. \quad (4)$$

and, finally, and crushing efficiency force given by

$$CFE = \frac{F_{av}}{F_{max}}. \quad (5)$$

The ideal crash structure should have a CFE close to unity, where the initial peak force is close to the mean force along the crushing time. If the average force is as high as the peak force, the energy absorption will be very satisfactory, because the area under the graphic is maximized. A CFE close to zero represents not only a initial large deceleration that can be harmful for the vehicle occupants but also a low energy absorption.

2.3. Material Law

The material law to be used depends on the initial considerations and its applicability along the project. Thus, the chosen model must perform the best approximations in all stages of material deformation in order to have satisfactory results.

The elastic behaviour is common across all models being defined by the Hooke's Law [4]. Analysing the models provided by $Altair^{®}RADIOSS^{®}$, the Johnson Cook Material Law [4] has proven to be effective to model the material for the crash tests.

This material law has in consideration the effect of the strain rate and the temperature. This formulation is valid for shell elements, truss and beams elements, which will be the case of the structure to be studied.

The stresses during the plastic deformation can be described by

$$\sigma = (a + b\varepsilon_n^p)\left(1 + c\ln\frac{\dot{\varepsilon}}{\dot{\varepsilon_0}}\right)\left(1 - T^{*^m}\right), \quad (6)$$

where σ is the flow stress, ε the plastic strain, a the yield Stress, b the hardening modulus, n the hardening exponent, c the strain rate coefficient, $\dot{\varepsilon}$ the strain rate, $\dot{\varepsilon_0}$ the reference strain rate and T^* the temperature exponent.

Analysing equation (6), the flow stress is influenced by three parameters: plastic strain, strain rate and temperature. Although, a simplification can be made to remove the temperature and strain rate effect in order to achieve quicker but reliable results. Regarding the strain rate effect, Chen et al.[5], concluded that several aluminium alloys can be modelled as strain rate insensitive. The tests will be performed at room temperature (298 K) so temperature effects can be neglected. Concluding, the final formula to model the material behaviour during the plastic formulation can be approximated as

$$\sigma = (a + b\varepsilon_n^p). \quad (7)$$

2.4. Heat Affected Zone

The Heat Affected Zone (HAZ) has special importance when several components of a structure are welded. When the joint is made, the band of material near the melting zone is highly affected promoting a degradation of its mechanical properties. The micro structural alterations are the main explanation to the changes in the macro characteristics of the material such yield stress and brittleness.

For several aluminium 5xxx and 6xxx series alloys, the reduction of the properties can be from 30% to 50% when joined by fusion welding [6]. With this high percentage, the heat effect cannot be neglected.

2.5. Finite Elements Analysis

The finite element method became the main analysis tool in the field of structural engineering. With the development of larger and faster processing capacities, the efficiency between reliable results and processing time has highly increased.

Firstly, it is necessary to understand if the analysis will be linear or non linear. In a linear analysis, it is assumed that the material will always be below the yield point, presenting an elastic regime. This type of analysis is the lighter solution in terms of computational effort. As previously mentioned, crash systems are made to absorb energy in the plastic regime, i.e., the material is always beyond the yield point. With this, it is concluded that the best analysis to be made will be non-linear, which manages to cover large deformations such as those the vehicle is subjected during impact [7].

In a crash scenario, the problem needs a solution of the type $\sum F = ma$. The initial velocity and the inertial forces have a high contribution for the solutions. The best approach for an impact scenario is an explicit dynamic analysis. In an explicit analysis, the results are computed at each time-step based on the previous time-step. This approach is used when the material behaviour is highly non linear and if the number of elements is too high. Furthermore, the explicit analysis is very efficient in cases where there are many contacts and elements. Comparing with an implicit analysis, it does not require large amounts of memory and CPU, since the results are analysed incrementally.

2.6. Multi-objective Optimization Algorithms

In the case of optimization in crashworthiness area, the ideal is to maximize the SEA and the CFE simultaneously. This way, the choice of an effective algorithm that deals with several objective functions is naturally important. The multi-objective optimization functions deal with with multiple functions that are usually conflicting with each other. Thus, there should be a compromise between the ideal value of the functions. This problem exists because it is expected that a maximization in one objective causes a detriment in the other objectives. The typical formulation for a multi objective problem is given by

$$\left.\begin{array}{lcl} Minimize/ & f_m(\boldsymbol{x}), & m = 1, 2, ..., M; \\ Maximize & g_j(\boldsymbol{x}) \geq 0, & j = 1, 2, ..., J; \\ subject\ to & h_k(\boldsymbol{x}) = 0, & k = 1, 2, ..., K; \\ & x_i^{(L)} \leq x_i \leq x_i^{(U)}, & i = 1, 2, ..., n. \end{array}\right\} \quad (8)$$

It is always necessary to define the M objective f functions corresponding to the expressions that will be maximized or minimized. If the optimization formulation is constrained, the equality and inequality functions, $h(x)$ and $g(x)$, are evaluated, as well as the upper and lower bounds, $x_i^{(L)}$ and $x_i^{(U)}$.

If a solution does not fit the domain defined by the constraint functions $g(x)$ and $h(x)$, it is called *infeasible solution*. The unique relevant solutions to the optimization problem will be the *feasible solutions*, that satisfy the constraint functions [8].

According to Deb [8] it is possible convert any minimization problem to a maximization problem and vice versa multiplying any objective function by -1. Similarly, the inequation $g(x)$ can be changed from a function "minor than" in "major than" the same way.

The NGSA II implemented by the function *gamultiobj* in $MATLAB^{®}$ determines at each iteration the individuals with lower rank. This parameter is defined as the set of non dominated solutions by their neighbours. A lower rank implies a better chance to pass the correspondent solution for the next generations. This way, it is ensured that the

best solutions are passed through the next generations. From the control made by the initial parameters it is possible to achieve a better convergence of the Pareto front. These parameters are the population size, the number of generations and the stopping criteria.

3. Implementation

The different considerations such as the materials, signal filtering, the mesh convergence, the inclusion of the heat affected zone and the software used to build the optimization procedure have to be studied before the optimization to obtain reliable results.

3.1. Material Selection

The material characteristics to take into account when a crash system is being built are the capacity to absorb energy, its durability and the ease of fabrication. Due to manufacturing constraints, stamping process is not possible, so the choice is to produce the components by simpler processes. Thus, it was concluded that the best choice to achieve design objectives is the aluminium.

Aluminium extrusions allow to produce almost any cross section design [9]. The shaping capacity with the cost-efficiency and the ease to riveting, welding, brazing or soldering makes this material ideal to make the structure. The resistance to corrosion comes from the fact that when the raw aluminium surface is exposed to air, a layer of aluminium oxide is created giving the material a high natural resistance [10].

The different types of aluminium alloys are referred in European Standards by four digits according to its constitution. The most common used alloys in automotive industry are the 6xxx and 7xxx. However, the 6xxx alloys are more easily extruded than 7xxx [9].

Thus, the characteristics of the materials chosen to perform the numerical simulations are in table 4. The main characteristics such as Yield Strength (YS), Ultimate Tensile Strength (UTS) and Elongation at break (A) of each alloy are given as well as the respective values for the HAZ.

Table 4: Selected materials for optimization comparison (adapted from [11])

Material	YS (MPa)	UTS (MPa)	A %	YS - HAZ (MPa)	UTS - HAZ (MPa)
6060 T64	120	180	12	60	100
6061 T4	110	180	15	95	150
6061 T6	240	260	8	115	175
6082 T6	250	290	8	125	185

The 6060 T64 and 6061 T4 alloys have a lower yield strength but a higher ductility, while the 6161 T6 and 6082 T6 alloys have the inverse characteristics. These choices were made to provide a wide range of solutions and have the perception of which properties have the major influence in the final results. With different characteristics, it is expected a wider spread in Pareto solutions.

3.2. Optimization Procedure

In this section it will be explained the optimization process for both structures. In order to achieve final results, several steps were performed from the creation of geometry to the analysis of final results by the developed script. The operation of this script is explained in figure 1.

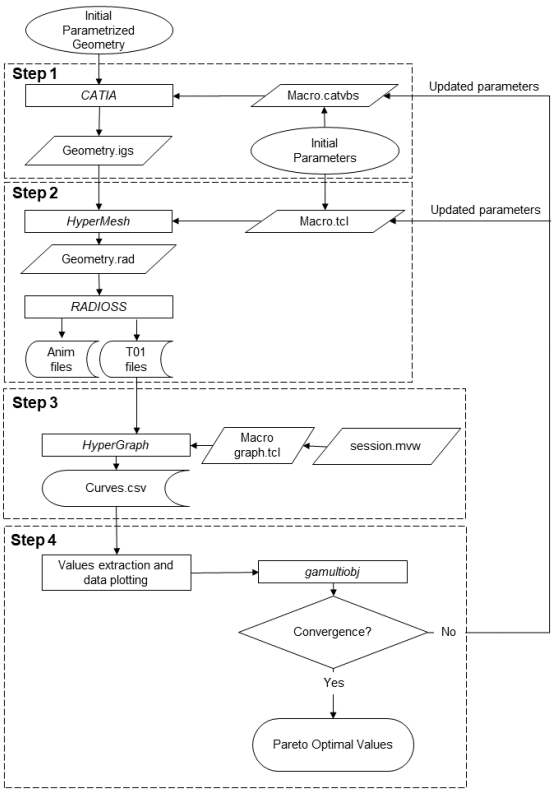

Figure 1: $MATLAB$ script flowchart

In order to execute the programs in the optimization procedure, the *dos* function from $MATLAB^{®}$ was used to pass the arguments to the windows command line to run the applications.

In **Step 1**, $CATIA^{TM}$ macro is modified depending on the parameters to be changed in the geometry. Then, the *dos* function runs the program in batch mode (without graphical interface) to have a faster execution. Additionally, in the *.catvbs* macro it is expressed the export of the *.igs* geometry that will be imported by $HyperMesh^{®}$ afterwards.

In **Step 2**, $HyperMesh^{®}$ is then executed, being passed by argument the macro with the changed parameters. Thus, a *.rad* is exported and read by $RADIOSS^{®}$. In this stage, the solution is computed. After the computation, the $TFILE$ and animation files are exported.

In **Step 3** the curves from simulations are obtained and the *.tcl* macro is executed by

HyperGraph® on the command line. The export is then done in *.csv* format and the resulting curves are then analysed by the *MATLAB*® script.

In **Step 4**, the *gamultiobj* algorithm evaluate the values obtained in each simulation. In case of no convergence, new parameters are created, being passed to the initial macro to be read by *CATIA* until the convergence is achieved. In case of convergence, the Pareto is shown, representing the optimal values for the optimization.

3.3. Geometry Parametrization

The initial geometry for analysis and optimization was designed in a parametrized way. The parameters that can be changed in a file with one structure and both structures are presented in figure 2 as well as a brief explanation in table 5.

Table 5: Description of the parameters used to build the geometry

Parameter	Description
t	thickness
tl	total length
tw	total width
bh	height of the bumper
lc	length of the crash box side
rb	bumper radius
lb	width of the bumper
dcb	distance between crash boxes
d	distance between structures

Both files are parametrized in the same way. The difference is in the parametrization of the file with both parts. In this case, the parameters of the primary structure are fixed to the values obtained in the respective optimization. Only the values for the secondary structure are modified in the macro as well as the distances between the structures d.

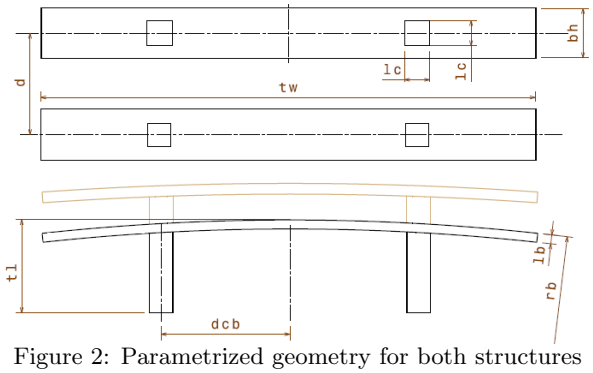

Figure 2: Parametrized geometry for both structures

3.4. Mesh Convergence

In an explicit simulation, the mesh size is exponentially correlated with the simulation effort. A reduction in the element size leads to a reduction in the time step and so the solver has to make not only more iterations but also more calculations due to the increase in elements number. In order to evaluate the effects between different time steps and mesh sizes, a single geometry was created to perform several impact tests to have a comparison basis. The 8mm mesh revealed the best compromise between reliable results and computational time.

3.5. HAZ Comparison

The weld zones were evaluated regarding heat effects in order to percept the effect on the overall performance of the structure. Kokkula et al. [12] included this effect in numerical simulations, showing a peak force reduction. This way, a FEA was made to understand the heat influence in these type of structures.

Thus, the elements in the junction between the crash box and the bumper were selected to define the HAZ properties. The figure 3 shows the selected elements.

Figure 3: Bumper with the Heat Affected Zone (blue) and unchanged properties (yellow)

The thickness was defined as constant and the 6061 T6 material properties was assigned as in table 4. The parameters respecting table 5 used to design the geometry in figure 3 are summarized in table 6.

Table 6: Geometry parameters for HAZ comparison

Parameter	t	lc	tl	tw	rb	dcb
Size (mm)	3.5	90	250	1250	9000	650

To compare the structures with the HAZ modelled or non modelled, it was made a crash test against a rigid wall with an imposed mass of 600 kg and with an initial velocity of 13.8 m/s. From the Force vs Displacement curves for both structures it was possible compare the effects. The obtained curves are in figure 4.

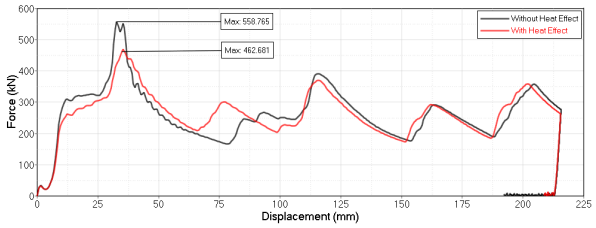

Figure 4: Force-displacement curve for a structure with and without HAZ effect

Thus, comparing both curves it is understandable a reduction of the maximum peak force in the structure with the HAZ modelled. This consideration implies an improvement in the global results since the CFE is dependent from the maximum peak force and the average force, i.e, as both these parameters are close from each one, the CFE value

will increase. Furthermore, the SEA value is not affected because the mass is equal on both structures. The reduction of the maximum peak force is mainly due to the yield stress reduction in the HAZ, causing the structure to deform in this area with a lower applied force. Concluding, the HAZ revealed a significant impact in the final results, making its modelling to be taken into account.

4. Results

Applying the *gamultiobj* from *MATLAB* referred on in section 2.6, the optimizations were made always with the purpose to comply the Euro NCAP regulations regarding the full width impact test protocol presented in section 2.1.

According to Campos et al. [13], the percentage of energy that has to be absorbed by the front structures must be 50 % of the total energy in the first half of the frontal structure in a vehicle.

Thus, the masses to be imposed in each case for the optimization procedure are in table 7.

Table 7: Different masses applied for structures optimization

Vehicle	Micro Car	Sports Car	Be 2.0	Big Sedan
Mass (kg)	1200	1,400	1,600	1,800
Mass RB (kg)	600	700	800	900

Following the Euro NCAP regulations, the initial velocity to be imposed will be 13.8 m/s as presented in table 7.

Thus, the energy absorbed by the structure has to be equal to the kinetic energy relative to the imposed initial conditions. The initial kinetic energy for each case is given by

$$E_c = \frac{1}{2} \cdot M_{RB} \cdot V^2. \tag{9}$$

For the primary structure, corresponding to the geometry to be implemented in the Micro Car, only the values of t, tl and lc were considered for optimization. The fixed values for the other parameters are in table 8.

Table 8: Fixed parameters for the primary structure

Parameter	rb	lb	bh	dcb	tw
Size (mm)	9000	25	100	650	1250

To optimize the secondary structures, it were considered the values of t, lc tl rb bh and lb. The fixed values of dcb and tw were the same as the primary structure. The value of d was set as 400 mm.

4.1. Crash box shapes

It was decided to use only simple shapes to prevent errors in meshing, reduce the generated elements, minimize costs and to ease the parametrization between different geometries but with reliable results. The shapes and the parametrization for lc value are represented in figure 5, where letter S, C and H will designate the quadrangular, circular and hexagonal shapes, respectively.

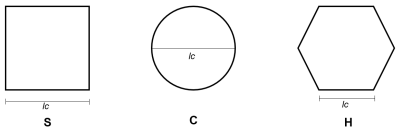

Figure 5: Crash box shapes for optimizations

4.2. Optimization of structures

The non linear constraints were defined through the Euro NCAP regulations. These conditions are evaluated by *gamultiobj* at each calculation as

$$\begin{cases} a_{3ms} - 65 \leq 0 \\ HIC_{15} - 700 \leq 0 \\ a_{max} - 80 \leq 0 \end{cases}, \tag{10}$$

where the values are in accordance with table 3.

To find the best design for the structures, 12 optimizations for each vehicle were performed corresponding to the 3 cross shapes shown in figure 5 and the 4 chosen materials.

With the previous considerations, the optimizations for the structures were performed. To find the optimum structure to absorb the correspondent energy given by equation (9) for each vehicle, several Pareto sets were analysed. The results presented in figure 6 represent the junction between the simulations for each crash box with the same material in the primary structure optimization. The same procedure was used to select the optimized structures in the other cases. The plots are organized in the configuration explained in tables 9 and 10. The *infeasible* solutions are not represented in this document since they do not have major relevance in the final results.

Table 9: Color code for each type of material

Material	6060 T64	6061 T4	6061 T6	6082 T6
Color	red	blue	green	magenta

Table 10: Symbol for each type of cross shape

Cross Shape	Q	C	H
Symbol	□	•	⬡

4.3. Micro Car

The selected values present in Pareto front to make a comparison to achieve the primary structure are in figure 6.

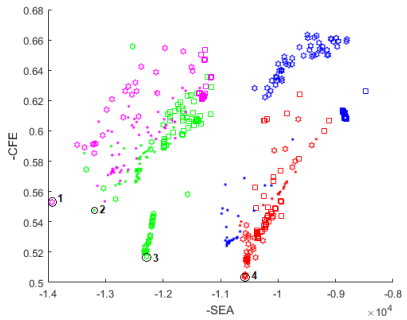

Figure 6: Final solutions for the primary structure

As seen in figure 6, there are four solutions that can be chosen to make the comparison.

Table 11: Obtained values for selected points for the primary structure

Point	CFE	SEA (J/kg)	Mass (kg)	HIC_{15}	a_{3ms} (g)	a_{max} (g)	δ (mm)
1	0.447	13930	4.105	220.7	53.4	61.2	261.1
2	0.452	13190	4.379	233.2	57.1	60.4	259.4
3	0.483	12286	4.664	232.8	55.9	56.4	248.6
4	0.496	10574	5.424	166.9	48.7	53.8	258.6

To select the best primary structure, it is necessary to evaluate the resultant force vs displacement curves in order to have the perception about the behaviour of the different solutions during impact. The obtained curves by the selected structures are presented in figure 7.

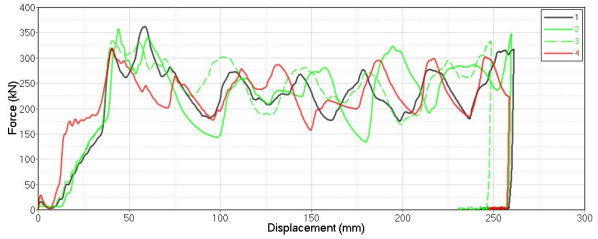

Figure 7: Force vs displacement curves for the selected solutions in the primary structure optimization

Analysing the figure, it can be seen that all the curves have the same pattern and the maximum displacements are almost equal. The parameters values for each structure are shown in table 12.

Table 12: Variable values for chosen points in the primary structure optimization

Point	Cross Shape	Material	t (mm)	lc (mm)	tl (mm)
1	H	6082 T6	3.7	30.1	318.7
2	C	6161 T6	3.6	79.7	306.3
3	H	6161 T6	4.2	29.6	318.3
4	H	6060 T64	4.0	54.7	319.3

By the values obtained and subsequent information it is possible to verify that the best choice to the primary structure is the point 1. Besides being the structure with smaller mass, it has the same length as the others. On other hand, a lower thickness eliminates the risk of oversize the structure. This way, the designed structure will always deform easily, avoiding damage to the structures behind the bumper in case of impact with a lower speed. Concluding, the chosen geometry to be the primary structure are represented in figure 8.

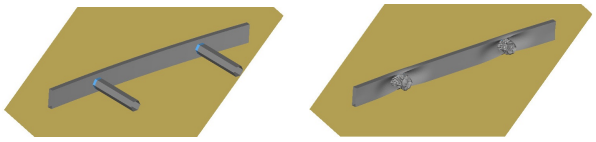

(a) Primary structure (b) Deformed primary structure

Figure 8: Optimized primary structure

4.4. Secondary structures

As stated previously, to find the best geometry to be used as secondary structure, the optimization will be performed always in parallel with the same primary structure for every vehicle typology. The approach used to optimize the geometries was the same as that of the primary structure. To find a structure to fulfill the requisites, the three different cross shapes given in figure 5 and the four materials were combined and the best solutions were chosen. The process to chose the best solution was the same as for primary structure. This way, analysing the values of the mass, HIC, a_{3ms}, a_{max} and δ, the structures were chosen with the respective values summarized in tables 13 and 14.

Table 13: Selected solution from the Sports Car structure optimization

Vehicle	CFE	SEA (J/kg)	Mass (kg)	HIC_{15}	a_{3ms} (g)	a_{max} (g)	δ (mm)
Sports Car	0.495	9945	6.728	245.7	54.0	55.2	239.3
Be 2.0	0.485	10581	7.221	264.0	55.9	56.6	253.5
Big Sedan	0.520	11398	7.545	188.0	48.2	52.5	247.9

Table 14: Variable values for the chosen point in the Sports Car optimization

Vehicle	Material & Shape	t (mm)	lc (mm)	tl (mm)	rb mm)	bh (mm)	lb (mm)
Sports Car	6061 T6 H	2.0	30.1	283.4	4747.1	56.2	20.6
Be 2.0	6082 T6 H	2.0	41.1	271.9	5608	59.5	23.0
Big Sedan	6082 T6 H	2.4	43.9	304.4	4627	56.5	24.4

4.5. Final Comparisons

Finally, it is then possible to verify the efficiency of the structures obtained comparing the final geometries for each case. Thus, analysing tables 15 and 16 it is possible to compare the energy absorption as well as the maximum peak force and the mass for each CMS. In the case of the vehicle typology with both structures the letters P, S and T represent the primary, secondary and both structures, respectively. The difference of the values respecting energy absorption or mass represented in table 16

is given by the quotient between the values of both structures for each case relative to the Sports Car.

Table 15: Micro Car optimized structure

Structure	F_{max} (kN)	a_{max} (g)	EA (J)	Mass (kg)
Primary	362.1	61.1	56979	4.105

Table 16: Secondary optimized structures

Vehicle	**Sports Car**		
Structure	**P**	**S**	**T**
F_{max}	352.3	134.4	381.6
a_{max}	50.9	19.4	55.1
Mass (kg)	4.105	2.623	6.728
Difference_{Mass}			
EA (J)	52113	15390	67502
Difference_{EA}			
Vehicle	**Be 2.0**		
Structure	**P**	**S**	**T**
F_{max}	348.7	180.2	457.0
a_{max}	44.1	22.8	57.8
Mass (kg)	4.105	3.116	7.221
Difference_{Mass}			+7.3 %
EA (J)	54604	22463	77071
Difference_{EA}			+14.2 %
Vehicle	**Big Sedan**		
Structure	**P**	**S**	**T**
F_{max}	351.6	212.9	555.0
a_{max}	39.5	23.9	62.4
Mass (kg)	4.105	3.440	7.545
Difference_{Mass}			+12.1 %
EA (J)	52800	33808	86607
Difference_{EA}			+28.3 %

In order to have a better perception about the behaviour of the structures, figure 9 was made to explicit the differences between the energy absorption and the peak force for each case.

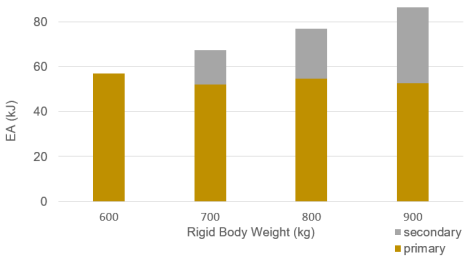

Figure 9: Energy absorption comparison

Analysing the tables and figures, it is possible to conclude that the primary structure absorbs almost the same energy in the different crash tests. This comes from the fact that the initial geometry is not oversized for the condition established in the 600 kg test. Thus, in the tests with a heavier vehicle, the structure is totally deformed, absorbing the energy that are supposed to. This phenomenon was predicted in the initial objectives, being accomplished in all optimized structures.

Moreover, the peak force is not directly related with the vehicle's mass neither with the sum of the peaks from the primary and secondary structure. The peak force from both structures do not occur at the same. However, if the objective of this project was to study a single structure to absorb the energy for each case, this parameter would be critical.

Furthermore, the maximum peak for each structure must be taken into account in the next vehicle design phase. The structures that will support the crash management systems have to be strong enough to carry the maximum forces imposed in the crash tests or, in an extreme case, to begin the deformation after the entire crush of the absorbing structures.

Moreover it can be stated that with an increase of 7,3 % and 12,14 % in mass, the absorbed energy increased 14,18 % and 28,3 % making the comparison between the Be 2.0 and Big Sedan values relative to the Sports Car, respectively. This way, the secondary structure implementation revealed a successful approach to fulfill the requisites. Finally, the final optimized geometries are shown in figures 10, 11 and 12. The structures are always designed with the darkest grey for the primary structure and the lighter for the secondary structure.

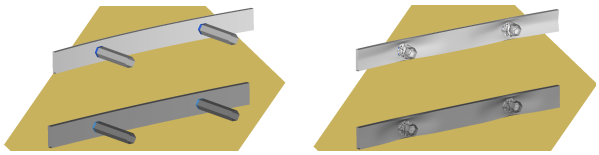

(a) Primary and secondary structures (b) Deformed primary and secondary structures

Figure 10: Optimized Sports Car structures

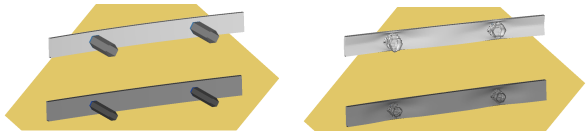

(a) Primary and secondary structures (b) Deformed primary and secondary structures

Figure 11: Optimized Be 2.0 structures

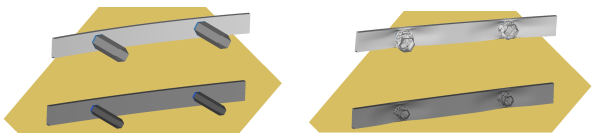

(a) Primary and secondary structures (b) Deformed primary and secondary structures

Figure 12: Optimized Big Sedan structures

Analysing the figures, it is noticeable the increase of robustness of the structure from the lighter to the heavier vehicle. This confirms the assumptions defined throughout the project. For the most demanding tests, it is necessary a structure with more material to absorb the additional kinetic energy that results from the impact.

Concluding, the primary and secondary structures have proven to be effective in the vehicle protection, overcoming the imposed constraints from the Euro NCAP regulations regarding full width frontal impact.

4.6. Computational Cost Assessment

The obtained solutions required a large computational effort. Table 17 shows the different times that took to optimize each structure. The values presented for the simulation time are an approximation since each simulation have a different time to solve due to the difference in elements number.

Table 17: Simulation time for each optimization

Vehicle	Simulation time (min.)	Number of simulations	Total time (min.)
Mini Car	15	828	12420
Sports Car	27	1272	34344
Be 2.0	27	1295	34965
Big Sedan	27	1235	33345

Concluding, the total computational time to make the calculations was estimated in $12420 + 34344 + 34965 + 33345\ min. = 115074\ min. = 79.9\ days$ which was possible thanks to the two computers available at the time of this work.

5. Experimental Validation Procedure

The final results and the material model must be validated to ensure the reliability of the process and the solutions. This way, a tensile test must be performed to identify the real characteristics of the material to be used and compare the material formulation with the experimental results. During the course of the project, it was not possible to acquire the material, so this chapter will serve to indicate what kind of tests and procedures have to be performed to implement the achieved solution in a real context.

5.1. Material Validation

The validation of the material is performed by an uni-axial or biaxial tensile test in order to find the stress vs strain curve. In the context of this work, the best approach would be to compare the curves from the four materials. The HAZ do not need to be checked in this phase because the effects of soldering can be studied in the full test model.

The test must be in accordance with the *ASTM B557M-15 - Standard Test Method for Tension Testing (Metric)* [14]. According to Nunes [15], it is possible to test the specimens in CEiiA installations with a servo-hydraulic MTS test machine with a 50 kN load cell (SN 429175) and a biaxial extensometer model 632.85F-05.

From the tests, several curves must be obtained for each material to compute the mean curve to minimize the errors in measuring. The main results from this test will be the Young's modulus, yield strength, Poisson's ratio and elongation at break, making possible the comparison between the theoretical prediction from the FE models and the real material.

6. Quasi-static Approximation

There is the option to use the servo-hydraulic MTS test machine with a 250 kN load cell (SN 10317357) present in CEiiA to validate the deformation pattern in the primary optimized structure. This way, it is necessary to verify if the quasi-static test have the same resultant characteristics as the dynamic. As the force required to perform the tests are almost the double of the maximum force given by the servo-hydraulic machine, a comparison with half of he structure was made to perceive the expected results in a quasi static test with half of the structure. For this purpose, three tests are made to find out the similarities between the two type of approaches.

Thus, two quasi-static tests are computed to compare with the dynamic test. The resultant curves from the simulations are in figure 13.

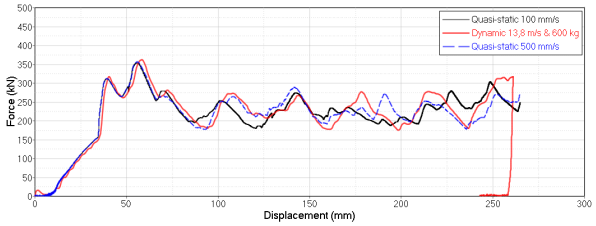

Figure 13: Trimmed curves force vs displacement for dynamic and quasi-static comparison

As seen, the values for each test are close to each other, so the quasi-static procedure can be a good approach to replace the dynamic test in an accessible place with the desired conditions. This way, the maximum force to perform the test in CEiiA installations has to be less than 250 kN. As seen in figure 13, this value is always exceeded. Thus, the solution is to perform the quasi-static test in half of the structure since it is symmetric.

The graphs from figure 14 were obtained to have the final comparison between tests with half and total structure.

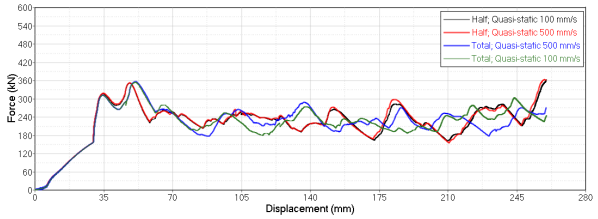

Figure 14: Comparison between the tests with the half and total geometry with trimmed curves

Analysing the figure 14 it is concluded that the tests to validate the solution for the primary structure can be made in CEiiA, since the values are close to the dynamic tests and the quasi-static tests with the total geometry.

7. Conclusions

The developed optimization process made possible to optimize different crash management systems to protect the occupants of four different vehicle typologies.

The process using a *MATLAB* script to implement the *NGSA II* optimization algorithm has proven to be a great approach to obtain the desired solutions. Beside, all solutions fulfills the Euro NCAP regulations regarding the full width frontal impact protocol.

The primary structure to be used in all vehicle topologies revealed the desired behaviour in all tests, protecting effectively the vehicle with lower mass.

Moreover, the optimized secondary structures to complement the primary structure in the heavier vehicles had a good relation between increase in mass and energy absorption.

The primary structure absorbed almost the same amount of energy in all tests, being the secondary structures responsible to absorb the energy remaining due to the mass addition.

The solutions in the Pareto front are mainly obtained by those made with the 6061 T6 and 6082 T6 alloys. It can be concluded that the value of the yield strength is the most important parameter with more importance for crashworthiness effects.

To achieve reliable results it was proved that the best approach is to compute the impact tests in the both structures simultaneously.

Finally, it is expectable that a quasi-static experimental test in half of the structure would be enough to validate the achieved solution for the primary structure.

Acknowledgements

I want to thank my supervisors, Professor André Marta and engineer Luís Colaço for their support during this project. Thanks to CEiiA and specially the mobility team for the availability and help whenever it was necessary. Finally, thanks to IST for the incredible experience during the last five years.

References

[1] European Commission Directorate General for Mobility and Transport. What are main crash injury situations? `https://ec.europa.eu/transport/road_safety/specialist/knowledge/vehicle/key_issues_for_vehicle_safety_design/what_are_main_crash_injury_problems_en`, Accessed April 2018.

[2] European New Car Assessment Programme (Euro NCAP). `https://www.euroncap.com/en`, Accessed September 2018.

[3] Tao Tang, Weigang Zhang, Hanfeng Yin, and Han Wang. Crushing analysis of thin-walled beams with various section geometries under lateral impact. *Thin-Walled Structures*, 102:43–57, 2016.

[4] Altair. Hyperworks 2017 Radioss User guide. `altairhyperworks.com`, Acessed June 2018.

[5] Y. Chen, A. H. Clausen, O. S. Hopperstad, and M. Langseth. Stress-strain behaviour of aluminium alloys at a wide range of strain rates. *International Journal of Solids and Structures*, 46:3825–3835, 2009.

[6] Pradeep Sensharma, Matthew Collette, and Joey Harrington. Effect of welded properties on aluminum structures. Technical report, Ship Structure Committee, 2010.

[7] Vince Adams and Abraham Askenazi. *Building Better Products with Finite Element Analysis*. OnWord Press, 1999.

[8] Kalyanmoy Deb. *Multi-Objective Optimization using Evolutionary Algorithms*. John Wiley & Sons, Ltd, 2001.

[9] European Aluminium Association. The Aluminum Automotive Manual. Applications - Car body – Crash Management Systems, 2013.

[10] Corrosion of Aluminum and Aluminum alloys. *ASM International*, pages 1 –10, 1999.

[11] The European Union. Eurocode 9: Design of aluminium structures, 2006. Part 1-1: General structural rules.

[12] S. Kokkula, O. S. Hopperstad, O. G. Lademo, T. Berstad, and M. Langseth. Offset impact behaviour of bumper beam-longitudinal systems: Numerical simulations. *International Journal of Crashworthiness*, 11(4):317–336, 2006.

[13] José Àngel López Campos, Abraham Segade Robleda, José Antonio Vilán Vilán, Paulino José García Nieto, and Javier Blanco Cordero. Study of a steel's energy absorption system for heavy quadricycles and nonlinear explicit dynamic analysis of its behavior under impact by FEM. *Materials*, 8(10):6893–6908, 2015.

[14] Standard Test Methods for Tension Testing Wrought and Cast Aluminum- and Magnesium-Alloy Products. *ASTM International*, 2015.

[15] Tiago Miguel Encarnação Nunes. Multi-objective design optimization of a frontal crash energy absorption system for a road-safe vehicle. Master's thesis, Instituto Superior Técnico, Portugal, 2017.